



Aryldiazenido ruthenium(II) complexes. Structure and characterization of *p*-tolyl diazenido ruthenium(II) complexes with pyrazole and imidazole ligands

J.G. Małecki*, I. Gryca, M. Penkala

Department of Crystallography, Institute of Chemistry, University of Silesia, ul. Szkolna 9, 40-006 Katowice, Poland

ARTICLE INFO

Article history:

Received 7 November 2012

Accepted 4 December 2012

Available online 2 January 2013

Keywords:

Ruthenium *p*-tolyl diazenido complexes

Pyrazole

Imidazole

X-ray

Electronic structure

Absorption and emission electronic spectra

DFT

ABSTRACT

The *p*-tolyl diazenido ruthenium(II) complexes $[\text{RuCl}_3(\text{PPh}_3)_2(\text{N}_2\text{PhCH}_3)]\cdot\text{CH}_3\text{OH}$ (**1**), $[\text{RuCl}_3(\text{PPh}_3)(\text{N}_2\text{PhCH}_3)(\text{HPz})]\cdot\text{CH}_3\text{OH}$ (**2**) and $[\text{RuCl}_3(\text{PPh}_3)(\text{N}_2\text{PhCH}_3)(\text{Im})]\cdot\text{CH}_3\text{OH}$ (**3**) were synthesized and characterized by IR, ^1H , ^{13}C , ^{31}P NMR, electronic absorption and emission spectroscopy, and X-ray crystallography. In the molecular structure of complex (**1**) some π – π stacking interactions are observed, whereas in the structure of the imidazole complex (**3**) graph set analysis shows intermolecular hydrogen bonded rings. The electronic structures of the complexes were calculated by DFT based on their crystal structures. The spin-allowed singlet–singlet electronic transitions of the complexes were calculated by time-dependent DFT and the UV–Vis spectra have been discussed on this basis. The emission properties of the complexes were also studied.

© 2012 Elsevier Ltd. All rights reserved.

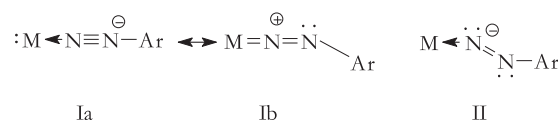
1. Introduction

Research involving ruthenium coordination chemistry incorporating various kinds of ligands has upsurged in recent years due to the fascinating reactivities exhibited by the resultant complexes [1]. Although most of the ligands containing azo nitrogen are multidentate (bi- or tridentate), the coordination mode of azo nitrogen to transition or non-transition metal ions is well documented [2–14]. Studies on the chemistry of ruthenium complexes with azo ligands have been ongoing and several interesting results related to electron transfer reactions, formation of metal–carbon bonds, aromatic ring amination, isomerism, cytotoxicity toward cancer cells, application in catalytic transformations and complexes with azo ligands that can act as a molecular switch, have been reported [15–23]. A significant property of the azo type ligands, due to the presence of the $-\text{N}=\text{N}-$ group, is that it may lead to the stabilization of low valent metal oxidation states. This is caused by its π acidity and the presence of low lying azo-centered π^* -molecular orbitals [24,25].

However most of the studied complexes containing the $\text{R}-\text{N}=\text{N}-\text{R}'$ type azo compounds as well as the aryldiazenido complexes have been overlooked in the literature. Nevertheless, some papers referred to aryldiazenido complexes of selected metals of groups 17, 18 and 19, i.e. Mn, Re and Ir [26–34]. Several reports on ruthenium aryldiazenido complexes have been released in the 1970s [35–40]. These studies concerned the synthesis and primary

spectroscopic characterization (IR, ^1H NMR). Indeed, the Cambridge Structural Database (CSD; ConQuest v. 1.14; 2012) presents only one structure of a ruthenium(II) phosphine complex with a *p*-tolyl azo ligand, published in 1973 [41].

Research on *p*-tolyl diazo complexes, especially ruthenium ones, concern the coordination geometries of the diazo ligand and its similarity to the nitrosyl group. The isoelectronic nature of NO^+ and the ArN_2^+ moiety allows the assumption that the coordinated aryldiazonium cation may also exhibit a duality of bonding modes. It can be characterized as either linear or bent $\text{M}-\text{N}-\text{N}$ structural units, as shown in scheme below:



Based on crystallographic evidence, it can be concluded that for describing the linear mode of bonding, the Ib unit is clearly more important than unit Ia. Similar studies extended by the dynamic behavior of aryldiazenido ligands in half sandwich ruthenium(II) complexes have been published in 2000 [42].

Nevertheless the reactivity of ruthenium aryldiazenido complexes has not been investigated yet. Moreover their electronic structures, bonding properties as well as absorption and emission electronic spectra have not been determined by density functional

* Corresponding author.

E-mail address: gmalecki@us.edu.pl (J.G. Małecki).

theory (DFT). Hence in this paper we report an experimental and quantum chemical study of ruthenium(II) *p*-tolylidiazenido complexes. Starting from the known $[\text{RuCl}_3(\text{PPh}_3)_2(\text{N}_2\text{PhCH}_3)]$ compound, reactions with pyrazole and imidazole, leading to the new complexes $[\text{RuCl}_3(\text{PPh}_3)(\text{N}_2\text{PhCH}_3)(\text{HPz})]$ and $[\text{RuCl}_3(\text{PPh}_3)(\text{N}_2\text{PhCH}_3)(\text{HIm})]\cdot\text{CH}_3\text{OH}$, have been performed. Quantum chemical studies, which include characterization of the molecular and electronic structures of the complexes by analyzing the optimized molecular geometries and electronic populations using the natural bond orbitals scheme, have been conducted. NBO analysis was also used to identify nature of the interactions between the azo ligand and the metal. The calculated density of states showed the interactions and influences of the orbital compositions in the frontier electronic structures. Finally, time dependent density functional theory (TD-DFT) was used to calculate and interpret the electronic absorption spectra.

2. Experimental

All reagents, except *p*-tolylidiazenido tetrafluoroborate, used for the syntheses of the complexes were commercially available and were used without further purification. The *p*-tolylidiazenido tetrafluoroborate was synthesized by standard diazotization of *p*-toluidine.

2.1. Synthesis of the complexes $[\text{RuCl}_3(\text{PPh}_3)_2(\text{N}_2\text{PhCH}_3)]\cdot\text{CH}_3\text{OH}$ (**1**), $[\text{RuCl}_3(\text{PPh}_3)(\text{N}_2\text{PhCH}_3)(\text{HPz})]$ (**2**) and $[\text{RuCl}_3(\text{PPh}_3)(\text{N}_2\text{PhCH}_3)(\text{Im})]\cdot\text{CH}_3\text{OH}$ (**3**)

Complex (**1**) was prepared according to the literature method [41] using CsCl instead of LiCl and has been obtained in almost quantitative yield. Complexes (**2**) and (**3**) have been synthesized as follows:

To a suspension of a 0.18 g sample of $[\text{RuCl}_3(\text{PPh}_3)_2(\text{N}_2\text{PhCH}_3)]\cdot\text{CH}_3\text{OH}$ in a 1:1 solution of methanol:acetone, 0.02 g of pyrazole or imidazole was added. In both cases, the mixture was refluxed for 3 h and then cooled down and filtered (the same products were obtained by stirring the reaction mixtures overnight). After standing overnight at room temperature, crystals suitable for X-ray crystal analysis were formed.

Complex (1): IR (KBr, cm^{-1}): 3056 ν_{ArH} ; 1889, 1868 $\nu_{(\text{N}=\text{N})}$; 1573 $\nu_{(\text{C}=\text{C})}$; 1482 $\delta_{(\text{C}-\text{CH in the plane})}$; 1434 $\nu_{\text{Ph(P-Ph)}}$; 1294 $\delta_{(\text{C}-\text{C toluidine})}$; 1052 $\delta_{(\text{CH}_3)}$; 816, 747 $\delta_{(\text{C}-\text{C out of the plane})}$; 695 $\delta_{(\text{C}-\text{C in the plane})}$; 520 $\delta_{(\text{ring})}$. ^1H NMR (400 MHz, CDCl_3) δ : 8.43–7.50 (m, *p*-toluidine, PPh_3), 7.47 (t, $J = 14.5$ Hz, *p*-toluidine, PPh_3), 7.43 (s, *p*-toluidine, PPh_3), 6.89 (d, $J = 8.1$ Hz, *p*-toluidine), 6.70 (d, $J = 8.2$ Hz, *p*-toluidine), 3.51 (s, methanol), 2.36 (s, *p*-toluidine), 1.42 (d, $J = 104.1$ Hz, methanol). ^{31}P NMR (162 MHz, CDCl_3) δ : 11.21 (s). ^{13}C NMR (101 MHz, CDCl_3) δ : 134.87 (t, $J = 5.1$ Hz, *p*-toluidine), 130.47–129.82 (m, PPh_3 , *p*-toluidine), 128.50 (s, PPh_3), 127.78 (t, $J = 4.9$ Hz, *p*-toluidine), 21.47 (s, *p*-toluidine). UV–Vis (methanol, $\log \epsilon$): 437 (1.29), 374 (2.31), 277 (3.77), 271 (3.98), 266 (3.76), 228 (4.34), 211 (4.88). Fluorescence ($c = 1 \times 10^{-4}$ mol/ cm^3 , methanol): exc: 258 nm; em: 288, 399 nm

Complex (2): Yield: 72%. IR (KBr, cm^{-1}): 3446, 3331 ν_{NH} ; 3058 ν_{ArH} ; 1876, 1858 $\nu_{(\text{N}=\text{N})}$; 1637 $\nu_{(\text{C}=\text{C})\text{PPh}_3}$; 1577, 1571 $\nu_{(\text{C}=\text{N/C}=\text{C})\text{HPz}}$; 1482 $\delta_{(\text{C}-\text{CH in the plane})}$; 1432 $\nu_{\text{Ph(P-Ph)}}$; 1183 $\delta_{(\text{C}-\text{C toluidine})}$; 1124, 1045 $\delta_{(\text{CH}_3)}$; 813, 777, 749 $\delta_{(\text{C}-\text{C out of the plane})}$; 695 $\delta_{(\text{C}-\text{C in the plane})}$; 520 $\delta_{(\text{ring})}$. ^1H NMR (400 MHz, CDCl_3) δ : 12.06 (s, NH), 8.26 (s, *p*-toluidine), 8.09–7.92 (m, PPh_3), 7.67 (s, PPh_3), 7.30 (dd, $J = 9.4, 4.5$ Hz, HPz), 7.11 (dd, $J = 23.9, 8.4$ Hz, HPz), 6.43 (s, *p*-toluidine), 2.36 (d, $J = 44.7$ Hz, $\text{CH}_3(\text{toluidine})$), 2.19 (s, CH_3OH). ^{31}P NMR (162 MHz, CDCl_3) δ : 24.43 (s, PPh_3). ^{13}C NMR (101 MHz, CDCl_3) δ : 143.27 (s, *p*-toluidine), 139.80 (s, HPz), 134.48 (d, $J = 9.2$ Hz, PPh_3), 131.08 (s, HPz), 130.45 (d, $J = 2.6$ Hz, PPh_3), 129.97 (s, *p*-toluidine),

128.62 (s, PPh_3), 128.00 (d, $J = 10.5$ Hz, *p*-toluidine), 120.20 (s, *p*-toluidine), 106.75 (d, $J = 3.5$ Hz HPz, *p*-toluidine), 21.63 (s, *p*-toluidine). UV–Vis (methanol, $\log \epsilon$): 421 (1.21), 304 (2.36), 275 (3.61), 267 (3.92), 261 (3.90), 212 (4.81). Fluorescence ($c = 1 \times 10^{-4}$ mol/ cm^3 , methanol): exc: 244 nm; em: 291, 385 nm.

Complex (3): Yield: 68%. IR (KBr, cm^{-1}): 3430, 3340 ν_{NH} ; 3056 ν_{ArH} ; 2961 ν_{CH_3} ; 1841 $\nu_{(\text{N}=\text{N})}$; 1622 $\nu_{(\text{C}=\text{C})\text{PPh}_3}$; 1576 $\nu_{(\text{C}=\text{N/C}=\text{C})\text{HIm}}$; 1483 $\delta_{(\text{C}-\text{CH in the plane})}$; 1434 $\nu_{\text{Ph(P-Ph)}}$; 1183 $\delta_{(\text{C}-\text{C toluidine})}$; 1091, 1066 $\delta_{(\text{CH}_3)}$; 815, 748 $\delta_{(\text{C}-\text{C out of the plane})}$; 695 $\delta_{(\text{C}-\text{C in the plane})}$; 520 $\delta_{(\text{ring})}$. ^1H NMR (400 MHz, CDCl_3) δ : 10.38 (s, HIm), 8.24 (s, *p*-toluidine), 7.98 (dd, $J = 10.7, 8.0$ Hz, PPh_3), 7.29 (d, $J = 7.6$ Hz, PPh_3), 7.10 (dt, $J = 37.7, 12.9$ Hz, HIm), 6.89 (s, HIm), 3.51 (s, CH_3OH), 2.42 (d, $J = 8.3$ Hz, *p*-toluidine), 2.19 (s, CH_3OH). ^{31}P NMR (162 MHz, CDCl_3) δ : 23.39 (s). ^{13}C NMR (101 MHz, CDCl_3) δ : 144.72 (s, *p*-toluidine), 134.52 (d, $J = 9.1$ Hz, HIm), 131.05 (s, *p*-toluidine), 130.77 (s, PPh_3), 130.28 (s, PPh_3), 128.53 (s, *p*-toluidine), 127.78 (s, HIm), 21.60 (s, *p*-toluidine). UV–Vis (methanol, $\log \epsilon$): 424 (1.24), 308 (2.34), 272 (3.67), 266 (3.97), 261 (4.01), 214 (4.78). Fluorescence ($c = 1 \times 10^{-4}$ mol/ cm^3 , methanol): exc: 243 nm; em: 293, 389 nm.

2.2. Physical measurements

Infrared spectra were recorded on a Nicolet Magna 560 spectrophotometer in the spectral range 4000–400 cm^{-1} using KBr pellets. Electronic spectra were measured on a Jasco V-600 spectrophotometer in the range 600–180 nm in methanol solutions. The ^1H , ^{13}C and ^{31}P NMR spectra were obtained at room temperature in CDCl_3 using a Bruker 400 MHz spectrometer. Luminescence measurements were made in methanolic solutions on an F-2500 FL spectrophotometer at room temperature.

2.3. Computational methods

The calculations were carried out using the GAUSSIAN09 [43] program. Molecular geometries of the singlet ground state of the complexes were fully optimized in the gas phase at the B3LYP/DZVP level of theory [44,45]. For each complex frequency calculations were carried out, verifying that the obtained optimized molecular structures correspond to energy minimum; thus only positive frequencies were found. The DZVP basis set [46] with *f* functions with exponents 1.94722036 and 0.748930908 was used to describe the ruthenium atom and the basis set used for the lighter atoms (C, N, Cl, P, H) was 6-31G with a set of “d” and “p” polarization functions. The TD-DFT method [47] was employed to calculate the electronic absorption spectra of the complexes using the solvent Polarizable Continuum Model (PCM). In this work 100 singlet excited states were calculated as vertical transitions for the complexes. Natural bond orbital (NBO) analysis was also made for all the complexes using the NBO 5.0 package [48] included in GAUSSIAN09. Natural bond orbitals are orbitals localized on one or two atomic centers which describe molecular bonding in a manner similar to a Lewis electron pair structure. They correspond to an orthonormal set of localized orbitals of maximum occupancy. NBO analysis provides the contribution of atomic orbitals (*s*, *p*, *d*) to the NBO σ and π hybrid orbitals for bonded atom pairs. In this scheme, three NBO hybrid orbitals are defined, namely bonding orbital (BD), lone pair (LP), and core (CR). They were analyzed for the atoms directly bonded to the ruthenium atom or presenting some kind of interaction with it. The contribution of particular groups (ligands, metal center) to a molecular orbital was calculated using Mulliken population analysis. GaussSum 2.2 [49] was used to calculate group contributions to the molecular orbitals and to prepare the partial density of states (DOS) spectra. The DOS spectra were created by convoluting the molecular orbital information with Gaussian curves of unit height and a FWHM (Full Width at Half Maximum) of 0.3 eV.

Table 1
Crystal data and structure refinement details of complexes [RuCl₃(PPh₃)₂(N₂PhCH₃)]·CH₃OH (**1**), [RuCl₃(PPh₃)(N₂PhCH₃)(HPz)] (**2**) and [RuCl₃(PPh₃)(N₂PhCH₃)(Im)]·CH₃OH (**3**).

	1	2	3
Empirical formula	C ₄₃ H ₃₇ Cl ₃ N ₂ P ₂ Ru,CH ₃ OH	C ₂₈ H ₂₆ Cl ₃ N ₄ PRu	C ₂₈ H ₂₆ Cl ₃ N ₄ PRu,CH ₃ OH
Formula weight	883.15	656.92	688.96
T [K]	295.0(2)	295.0(2)	295.0(2)
Crystal system	monoclinic	monoclinic	monoclinic
Space group	<i>P</i> 2 ₁ / <i>c</i>	<i>C</i> 2/ <i>c</i>	<i>P</i> 2 ₁ / <i>n</i>
Unit cell dimensions			
<i>a</i> (Å)	12.4604(6)	17.9994(4)	9.9120(3)
<i>b</i> (Å)	18.4627(9)	18.0599(3)	15.2795(4)
<i>c</i> (Å)	18.5702(8)	17.3058(4)	20.9555(7)
β (°)	92.577(4)	91.953(2)	96.075(3)
<i>V</i> (Å ³)	4267.8(3)	5622.3(2)	3155.90(17)
<i>Z</i>	4	8	4
<i>D</i> _{calc} (Mg/m ³)	1.374	1.552	1.450
Absorption coefficient (mm ⁻¹)	0.665	0.925	0.830
<i>F</i> (000)	1808	2656	1400
Crystal dimensions (mm)	0.15 × 0.06 × 0.04	0.23 × 0.09 × 0.03	0.20 × 0.11 × 0.03
θ range for data collection (°)	3.27–25.05	3.38–25.05	3.31–25.05
Index ranges	–14 ≤ <i>h</i> ≤ 14 –21 ≤ <i>k</i> ≤ 21 –22 ≤ <i>l</i> ≤ 22	–21 ≤ <i>h</i> ≤ 21 –21 ≤ <i>k</i> ≤ 21 –20 ≤ <i>l</i> ≤ 20	–11 ≤ <i>h</i> ≤ 11 –18 ≤ <i>k</i> ≤ 18 –24 ≤ <i>l</i> ≤ 24
Reflections collected	39482	25724	27220
Independent reflections	7528 [<i>R</i> _{int} = 0.0552]	4975 [<i>R</i> _{int} = 0.0252]	5571 [<i>R</i> _{int} = 0.0494]
Data/restraints/parameters	7528/0/481	4975/0/339	5571/0/362
Goodness-of-fit on <i>F</i> ²	1.041	1.035	1.029
Final <i>R</i> indices [<i>I</i> > 2 <i>s</i> (<i>I</i>)]	<i>R</i> ₁ = 0.0421 <i>wR</i> ₂ = 0.1010	<i>R</i> ₁ = 0.0267 <i>wR</i> ₂ = 0.0618	<i>R</i> ₁ = 0.0417 <i>wR</i> ₂ = 0.0758
<i>R</i> indices (all data)	<i>R</i> ₁ = 0.0572 <i>wR</i> ₂ = 0.1101	<i>R</i> ₁ = 0.0378 <i>wR</i> ₂ = 0.0657	<i>R</i> ₁ = 0.0671 <i>wR</i> ₂ = 0.0812
Largest difference in peak and hole (e Å ⁻³)	0.748/–0.401	0.703/–0.356	0.335/–0.363

2.4. Crystal structure determination and refinement

The crystals of [RuCl₃(PPh₃)₂(N₂PhCH₃)]·CH₃OH (**1**), [RuCl₃(PPh₃)(N₂PhCH₃)(HPz)] (**2**) and [RuCl₃(PPh₃)(N₂PhCH₃)(Im)]·CH₃OH (**3**) were mounted in turn on an Xcalibur, Atlas, Gemini Ultra Oxford Diffraction automatic diffractometer equipped with a CCD detector, and used for data collection. X-ray intensity data were collected with graphite monochromated MoK α radiation (λ = 0.71073 Å) at temperature 295.0(2) K, with the ω scan mode. Ewald sphere reflections were collected up to a 2θ value of 50.10. The unit cell parameters were determined from least-squares refinements of the setting angles of 11429, 9025 and 6984 strongest reflections. Details concerning crystal data and refinement are gathered in Table 1. Lorentz, polarization and empirical absorption corrections using spherical harmonics implemented in SCALE3 ABSPACK scaling algorithm [50] were applied. The structures were solved by the Patterson method and subsequently completed by difference Fourier recycling. All the non-hydrogen atoms were refined anisotropically using the full-matrix, least-squares technique. The OLEX2 [51] and SHELXS97, SHELXL97 [52] programs were used for all the calculations. Atomic scattering factors were incorporated in the computer programs.

3. Results and discussion

3.1. Spectroscopic characterization of the complexes

The *p*-tolylidiazenido ligands are characterized in the infrared spectra by strong bands with maxima in the range 1850–1900 cm⁻¹. The IR spectra of the starting complex (**1**), (**2**) and (**3**) present bands at (1889, 1868), (1876, 1858) and 1841 cm⁻¹, respectively. These frequencies are remarkable similar to the values of ν (NO) found for the analogous nitrosyl complexes. For comparison, in the IR spectrum of [RuCl₃(NO)(PPh₃)(HPz)] the nitrosyl stretching band is observed at 1879 cm⁻¹ [53]. However, some decreasing of the stretching frequencies from 1889 cm⁻¹ in the

parent complex (**1**) to 1841 cm⁻¹ in the imidazole one (**3**) suggests increasing population of the diazenido π^* orbital in the row of complexes (**1**), (**2**) and (**3**).

The ¹H, ¹³C and ³¹P NMR spectra of the complexes are given in Section 2. The signals in the proton and carbon NMR spectra are assigned to the *p*-tolylidiazenido, triphenylphosphine and diazole ligands, as seen in Section 2.1. In the phosphorus spectrum of the parent complex [RuCl₃(PPh₃)₂(N₂PhCH₃)]·CH₃OH (**1**), one signal (11.21 ppm) for the magnetically equivalent phosphorus atoms suggests the presence of two triphenylphosphine groups in perfect *trans* positions relative to each other. Incorporating the diazine ligands into the coordination sphere of the parent diazenido complex (**1**) gave monophosphine complexes for which the ³¹P NMR signals are shifted to lower fields, 24.43 and 23.39 ppm in the complexes with the pyrazole and imidazole ligands, respectively. The difference of approximately 1 ppm between δ (³¹P) in complexes (**2**) and (**3**) could be explained by the stronger π acceptor ability of 1,2- compared to 1,3-diazole occupying a *trans* position to the PPh₃ ligand. Hence a slightly greater deshielding effect is observed for pyrazole complex (**2**). Of course, at the same time, these data indicate a stronger σ donor property of the imidazole in the *trans* position.

3.2. Molecular structures

Crystals suitable for single crystal X-ray analysis were obtained by slow evaporation of the reaction mixtures. The complexes crystallize in the monoclinic system, *P*2₁/*c*, *C*2/*c* and *P*2₁/*n* space groups as solvates with one methanol molecule (**1** and **3**) and without solvent as complex (**2**). The molecular structures of the complexes are displayed as ORTEP representations in Fig. 1, and selected bond distances and angles are collected in Table 2. The crystal structure of complex (**1**) has been published earlier as an acetone solvate [41] and our results agree with those published earlier. The differences between the structures are visible in the N=N bond length (that reported earlier is shorter by 0.012 Å); moreover the Ru–N–N and N–N–Ar angles differ by about 1°. The structures of the complexes can

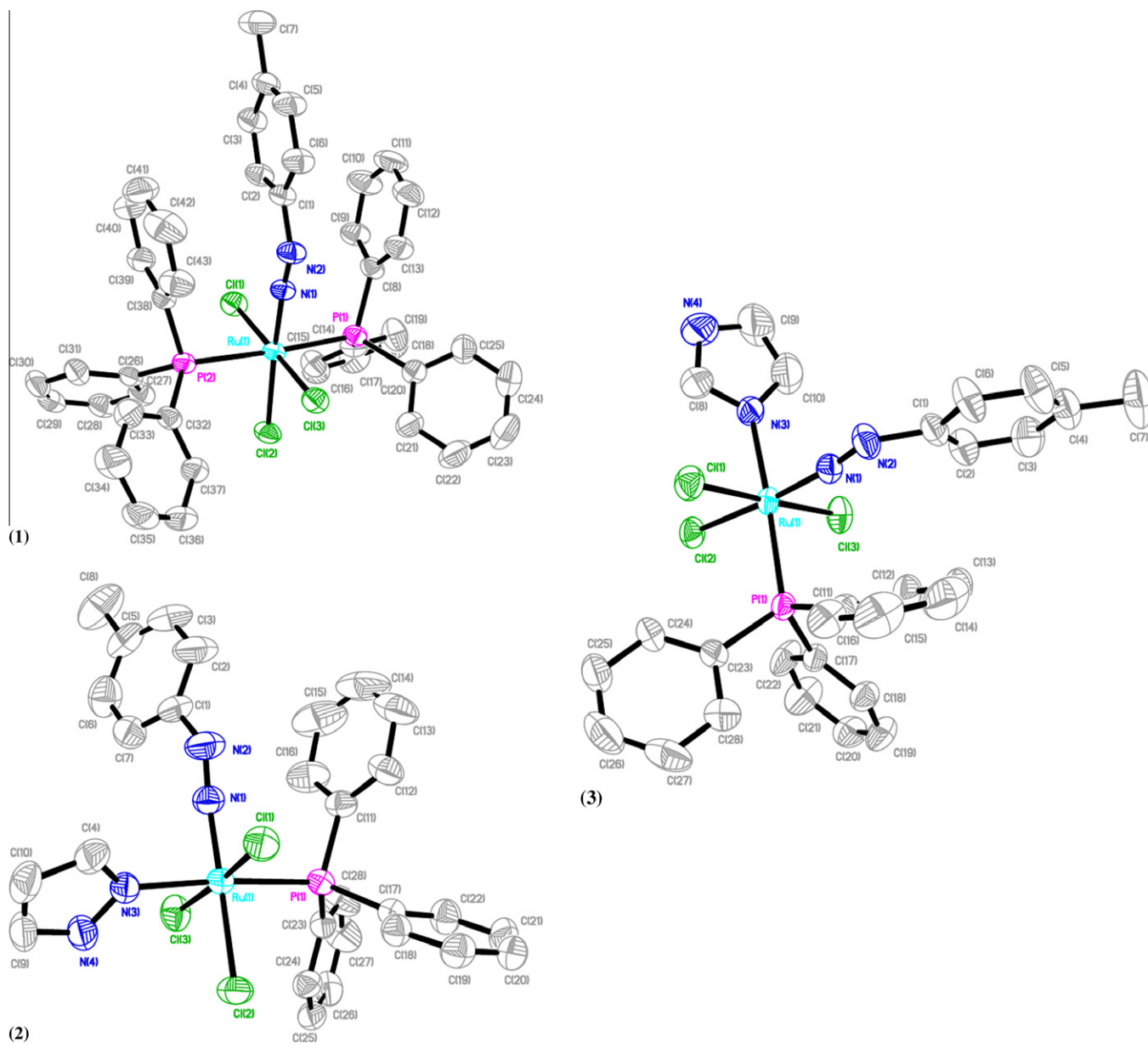


Fig. 1. ORTEP drawings of complexes $[\text{RuCl}_3(\text{PPh}_3)_2(\text{N}_2\text{PhCH}_3)] \cdot \text{CH}_3\text{OH}$ (**1**), $[\text{RuCl}_3(\text{PPh}_3)(\text{N}_2\text{PhCH}_3)(\text{HPz})]$ (**2**) and $[\text{RuCl}_3(\text{PPh}_3)(\text{N}_2\text{PhCH}_3)(\text{Im})] \cdot \text{CH}_3\text{OH}$ (**3**) with 50% probability displacement ellipsoids. Hydrogen atoms and methanol solvent molecules in complexes (**1**) and (**3**) are omitted for clarity.

be considered as distorted octahedral and the deviations from the expected bond angles do not exceed 5° (Table 2). The Ru–P distances in the *p*-tolylidiazenido complex (**1**), equal to 2.4378(11) and 2.4407(11) Å, fall in the range 2.41–2.44 Å observed for six-coordinate ruthenium(II) complexes containing mutually *trans* PPh_3 ligands. The ruthenium–PPh₃ bond distances have similar values in the complexes (**2**) and (**3**), but they are shorter by about 0.06 Å than those in (**1**). The enhancement of the Ru–P bond is probably due to weaker Ru–N(HPz/Im) backbonding than for the ruthenium–phosphine one. The Ru(1)–Cl(2) distances are noticeably shorter compared to Ru(1)–Cl(1)/(3) as a result of its *trans* position relative to the diazenido ligand. The *trans* effect of the aryldiazenido ligand resembles the effect caused by a linear nitrosyl moiety, but the shortening of the Ru(1)–Cl(2) bond presented in the pyrazole nitrosyl ruthenium(II) complex is larger than that observed in the complex (**2**). The π -acceptor nature of both diazenido and nitrosyl groups enhances the π -donation character of the ligands in the *trans* position which results in bond shortening in

the case of σ - and π -donor ligands, such as chloride. Moreover, the electronic properties of other ligands have an impact on the *trans* effect of the diazenido ligand, as can be seen in the data collected in Table 2. The Ru(1)–Cl(2) distance in complex (**2**) is shorter due to the stronger π -acceptor properties of the pyrazole ligand compared to the imidazole ligand. Thereby the Ru(1)–N(1) distance in the pyrazole complex (**2**) is slightly shorter by 0.004 Å. In the pyrazole complex (**2**) the N(1)–N(2) bond length is elongated compared with the parent complex (**1**) by about 0.013 Å, while in the imidazole complex (**3**) the elongation of the diazenido bond is negligible. The lengthening of the N–N bond and decrease of the Ru–N–N angle in the pyrazole complex (**2**) confirm a weaker backbonding interaction in complex (**2**) than in complex (**3**). However the comparison between complex (**2**) and its nitrosyl analog shows some elongation of the Ru–N₂PhCH distance compared to Ru–NO; 1.731(2) Å in $[\text{RuCl}_3(\text{NO})(\text{PPh}_3)(\text{HPz})]$ and 1.784(2) Å in $[\text{RuCl}_3(\text{N}_2\text{PhCH}_3)(\text{PPh}_3)(\text{HPz})]$. In both the nitrosyl and diazenido complexes the coordination modes are not perfectly linear. In

Table 2
Selected bond lengths [Å] and angles [°] of complexes [RuCl₃(PPh₃)₂(N₂PhCH₃)]·CH₃OH (**1**), [RuCl₃(PPh₃)(N₂PhCH₃)(HPz)] (**2**) and [RuCl₃(PPh₃)(N₂PhCH₃)(Im)]·CH₃OH (**3**).

	1		2		3	
	Exp	Calc	Exp	Calc	Exp	Calc
<i>Bond lengths [Å]</i>						
Ru(1)–N(1)	1.788(3)	1.80	1.784(2)	1.80	1.787(3)	1.80
Ru(1)–N(3)			2.144(2)	2.18	2.126(3)	2.19
Ru(1)–Cl(1)	2.3926(11)	2.49	2.3760(7)	2.41	2.3689(9)	2.39
Ru(1)–Cl(2)	2.3896(11)	2.43	2.3492(6)	2.38	2.3619(9)	2.44
Ru(1)–Cl(3)	2.3867(10)	2.42	2.4031(7)	2.50	2.3998(10)	2.47
Ru(1)–P(1)	2.4378(11)	2.51	2.3689(7)	2.43	2.3667(10)	2.43
Ru(1)–P(2)	2.4407(11)	2.51				
N(1)–N(2)	1.152(4)	1.17	1.165(3)	1.17	1.157(4)	1.18
<i>Angles [°]</i>						
N(1)–Ru(1)–Cl(1)	89.39(10)	91.8	87.15(7)	88.6	89.69(9)	88.9
N(1)–Ru(1)–Cl(2)	175.87(11)	175.7	177.24(7)	174.5	175.11(10)	175.2
N(1)–Ru(1)–Cl(3)	88.33(10)	86.3	91.94(7)	91.8	90.25(9)	91.1
N(3)–Ru(1)–Cl(1)			87.84(6)	88.7	88.97(9)	89.3
N(3)–Ru(1)–Cl(2)			86.79(6)	85.5	86.27(9)	85.4
N(3)–Ru(1)–Cl(3)			87.52(6)	87.5	89.84(9)	89.1
N(1)–Ru(1)–N(3)			91.39(9)	90.1	88.91(13)	90.0
Cl(1)–Ru(1)–Cl(2)	94.56(4)	92.5	90.71(2)	91.4	91.10(3)	90.5
Cl(1)–Ru(1)–Cl(3)	176.87(4)	178.2	175.25(2)	176.3	178.81(4)	178.4
Cl(2)–Ru(1)–Cl(3)	87.75(4)	89.4	90.05(3)	87.9	88.86(3)	89.3
N(1)–Ru(1)–P(1)	90.34(10)	91.6	92.98(7)	93.0	93.64(10)	93.3
N(3)–Ru(1)–P(1)			175.55(6)	176.7	177.16(9)	176.6
N(1)–Ru(1)–P(2)	90.34(10)	91.6				
Cl(1)–Ru(1)–P(1)	86.71(4)	88.4	93.23(2)	93.7	89.79(4)	90.2
Cl(1)–Ru(1)–P(2)	87.10(4)	88.4				
Cl(2)–Ru(1)–P(1)	88.71(4)	88.6	88.87(2)	90.1	91.19(3)	91.2
Cl(2)–Ru(1)–P(2)	91.04(4)	88.6				
Cl(3)–Ru(1)–P(1)	95.45(4)	91.7	91.48(2)	91.4	91.40(4)	91.3
Cl(3)–Ru(1)–P(2)	90.77(4)	91.7				
P(1)–Ru(1)–P(2)	173.76(4)	175.5				
Ru(1)–N(1)–N(2)	172.0(3)	178.1	169.4(2)	174.4	172.6(3)	174.3
N(1)–N(2)–C(1)	136.7(4)	136.6	133.5(3)	134.6	132.9(3)	133.4

the nitrosyl complex the Ru–N–O angle is 176.6(3)° and the *p*-tolyl diazo ligand is more bent with values of 169.4(2)° and 172.6(3)° in the complexes with pyrazole and imidazole, respectively. A comparison of the metric parameters of the nitrosyl and *p*-tolyl diazo pyrazole ruthenium(II) complexes shows both ligands as good π -acceptors, but the diazenido ligand seems to be weaker than NO, which is clearly visible in Fig. 3. Generally this fact comes from differences in the shortening of the ruthenium–chloride distance in the *trans* arrangement to the nitrosyl and diazenido ligands.

In the molecular structures of the complexes several inter- and intra-molecular hydrogen bonds [54] exist and details of these are collected in Table 3. In the crystal structure of the imidazole complex (**3**) graph set analysis [55] shows the dimeric form ($R_4^4(16)$) of the complex linked through methanol molecules, as is presented in Fig. 2. In the molecular structure of the parent complex (**1**) some π – π stacking between a PPh₃ phenyl and the phenyl ring of the *p*-tolyl diazenido ligand is also observable. The plane-to-plane distance between the phosphine phenyl centroid, determined by C(38)–C(43), and the C(1)–C(6) carbons of the N₂PhCH₃ ligand is equal to 3.933 Å, with the angle between the normal and the centroids being 9.75° and with a shift distance 2.22 Å. The P(1)–Ru(1)–P(2) angle in the complex of 173.76(4)°, lower than that for a linear arrangement, indicates geometrically non-equivalent phosphine moieties, though the presented π -stacking interaction may explain the singlet signal in the ³¹P NMR spectrum.

3.3. Quantum calculations

The ground states geometries of the complexes were optimized in singlet states using the DFT method with the B3LYP functional. The calculations were carried out for gas phase molecules without

solvent molecules in (**1**) and (**3**) and, in general, the predicted bond lengths are over-estimated by about 0.1 Å and the angles are almost unchanged. Nevertheless the general trends observed in the experimental data are reproduced in the calculations, as can be seen in the data collected in Table 2.

Based on the optimized geometries of the complexes, NBO analyses were performed in order to reveal the nature of the coordination mode between ruthenium and the donor atoms of

Table 3
Hydrogen bonds for complexes [RuCl₃(PPh₃)₂(N₂PhCH₃)]·CH₃OH (**1**), [RuCl₃(PPh₃)(N₂PhCH₃)(HPz)] (**2**) and [RuCl₃(PPh₃)(N₂PhCH₃)(Im)]·CH₃OH (**3**) (Å and °).

D–H...A	d(D–H)	d(H...A)	d(D...A)	∠(DHA)
1				
C(3)–H(3)...Cl(1) #1	0.93	2.82	3.533(5)	134.3
C(6)–H(6)...Cl(2) #2	0.93	2.82	3.562(5)	137.4
C(15)–H(15)...Cl(1)	0.93	2.71	3.309(5)	123.1
C(15)–H(15)...Cl(2)	0.93	2.68	3.358(5)	130.3
C(27)–H(27)...Cl(2)	0.93	2.67	3.447(5)	141.1
2				
N(4)–H(4)...Cl(3)	0.84(3)	2.66(3)	3.157(3)	119(3)
N(4)–H(4)...Cl(3) #3	0.84(3)	2.72(3)	3.375(3)	136(3)
C(18)–H(18)...Cl(1)	0.93	2.59	3.336(3)	137.9
C(24)–H(24)...Cl(2)	0.93	2.73	3.544(3)	146.9
3				
O(1)–H(1)...Cl(3)	1.02(9)	2.16(9)	3.161(4)	166(8)
N(4)–H(4)...O(1) #1	1.01(6)	1.87(6)	2.833(6)	159(5)
C(8)–H(8)...Cl(1)	0.93	2.81	3.247(5)	110.0
C(22)–H(22)...Cl(2)	0.93	2.68	3.519(4)	150.2
C(24)–H(24)...Cl(1)	0.93	2.77	3.285(4)	116.2
C(24)–H(24)...Cl(2)	0.93	2.66	3.427(4)	140.4

Symmetry transformations used to generate equivalent atoms: #1 1 – x, 1 – y, 1 – z; #2 1 – x, 1/2 + y, 3/2 – z; #3 1/2 – x, 1/2 – y, 1 – z.

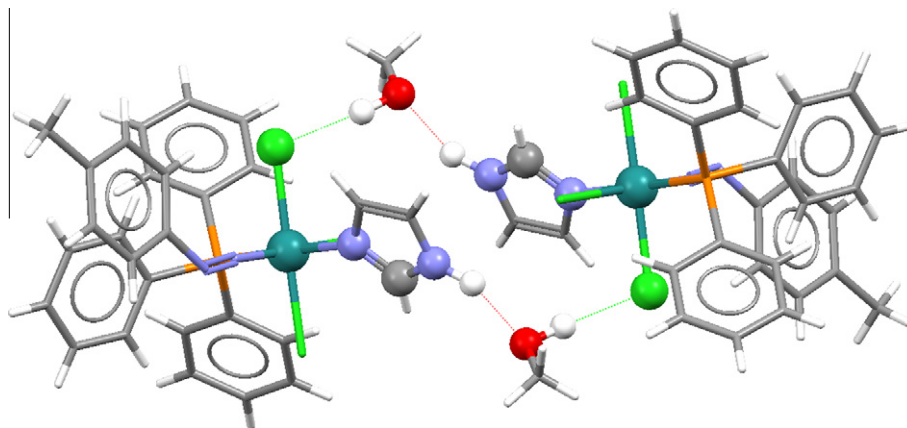


Fig. 2. The $Ru_4^+(16)$ motif in the crystal structure of complex (3).

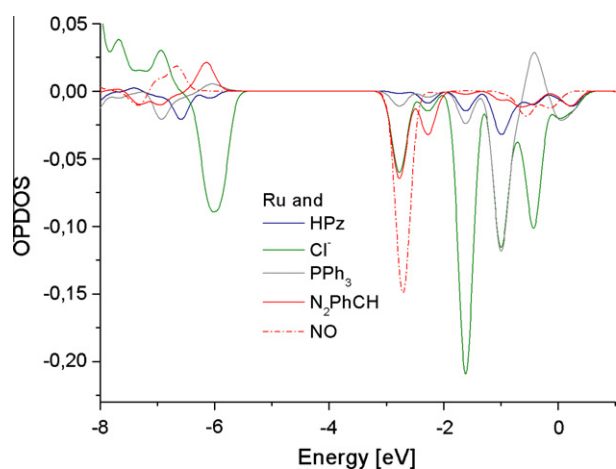


Fig. 3. The overlap partial density of states (OPDOS) diagram for the complex $[RuCl_3(PPh_3)(N_2PhCH_3)(HPz)]$ (2) with the ruthenium–nitrosyl ligand interaction in $[RuCl_3(PPh_3)(NO)(HPz)]$ (dash-dot line).

the ligands. These analyses showed that the bonding between the *p*-tolylidiazenido ligands and ruthenium is covalent; the calculated Wiberg bond's indices have values from 1.27 to 1.30 (Table 4). The highest value in the imidazole complex (3) suggests the strongest delocalization of π -electron density over the linear fragment $-N=N-$. For the diazenido group two natural bond orbitals for N–N, and two for the Ru–N bonds were detected. However participation of the *p* orbital in the hybrid describing the second Ru–N₂ bond is highest in the imidazole complex (3), as presented in Table 4. The Wiberg indices of ruthenium(II) and the pyrazole or imidazole nitrogen donor atom bonds are 0.436 and 0.431, respectively. These values indicate Coulomb-type interactions and confirm the higher donor properties of 1,3- (Im) than 1,2-diazole (HPz) ligands. The differences in the donor–acceptor properties of pyrazole and imidazole are stated in the natural charges on the ruthenium, being equal to -0.36 in (1), -0.11 in (2) and -0.41 in (3). The low charge in complex (2) confirms the strong π -acceptor property of pyrazole and at the same coincides with the weaker Ru–N_(HPz) backbonding interaction in complex (2) than in complex (3). Hence the natural charges on the $-N=N-$ part of the diazenido ligand decrease from 0.15 in (1) through 0.12 in (2) to 0.11 in (3). The Wiberg indices, equal to 0.8 for chloride in a *trans* position to the *p*-tolylidiazenido ligand and 0.7 for two mutually *trans* chloride ligands, also indicate the covalent character of the interaction between chloride and ruthenium in these complexes.

Table 4

The occupancies and hybridization of the calculated R–N and N–N natural bond orbitals (NBOs) of complexes $[RuCl_3(PPh_3)_2(N_2PhCH_3)]$ (1), $[RuCl_3(PPh_3)(N_2PhCH_3)(-HPz)]$ (2) and $[RuCl_3(PPh_3)(N_2PhCH_3)(Im)]$ (3).

BD (2-center bond)	Occupancy	Hybridization of NBO	Wiberg bond indices
<i>Ru–N(Ntolyl)</i>			
1	1.902 (0.218)	0.468 ($sp^{2.50}d^{2.99}$) _{Ru} + 0.884($sp^{0.61}$) _N	1.27
	1.887 (0.511)	0.744 ($p^{7.33}d^{66.81}$) _{Ru} + 0.668(<i>p</i>) _N	0.42
2	1.905 (0.231)	0.470 ($sp^{3.02}d^{3.55}$) _{Ru} + 0.883($sp^{0.61}$) _N	1.28
	1.884 (0.500)	0.732 ($p^{7.96}d^{65.16}$) _{Ru} + 0.681(<i>p</i>) _N	0.42
3	1.907 (0.228)	0.468 ($p^{3.07}d^{3.56}$) _{Ru} + 0.884($sp^{0.78}$) _N	1.30
	1.893 (0.478)	0.733 ($p^{7.26}d^{64.32}$) _{Ru} + 0.681(<i>p</i>) _N	0.42
<i>N–N</i>			
1	1.985 (0.068)	0.696($sp^{1.86}$) _{N(1)} + 0.718($sp^{1.14}$) _{N(2)}	2.01
	1.963 (0.409)	0.674(<i>p</i>) _{N(1)} + 0.738(<i>p</i>) _{N(2)}	
2	1.984 (0.087)	0.693($sp^{1.87}$) _{N(1)} + 0.721($sp^{1.11}$) _{N(2)}	1.99
	1.962 (0.399)	0.675(<i>p</i>) _{N(1)} + 0.738(<i>p</i>) _{N(2)}	
3	1.986 (0.016)	0.707($sp^{1.63}$) _{N(1)} + 0.707($sp^{1.64}$) _{N(2)}	1.98
	1.961 (0.401)	0.674(<i>p</i>) _{N(1)} + 0.734(<i>p</i>) _{N(2)}	

The natural population of the valence d_{Ru} orbitals in complex (1) (d_{xy} 1.71, d_{xz} 1.92, d_{yz} 1.15, $d_{x^2-y^2}$ 1.14 and d_z^2 1.20) corresponds rather to ruthenium(0). The sum of the $n(d_z^2)$ and $n(d_{x^2-y^2})$ values reflect the σ -donor properties of the ligands, and these are 2.34 in (1), 2.75 in (2) and 2.76 in (3), while the d_π occupancies (d_{xz} and d_{yz}) of 3.07 in (1) and (3) and 3.10 in (2), significantly lower than 4, suggest rather strong π -acceptor properties of the ligands surrounding the central ruthenium ion. The interaction of the ligands with the ruthenium atom in complex (1), presented in Fig. 3, clearly shows that the σ -donor property of the diazenido ligand is noticeable smaller than that of the chloride ligands, but it is similar to that of the triphenylphosphine ligand. The π -acceptor ability of N_2PhCH is emphasized in LUMO, LUMO+1 ($d_{x^2-y^2}$) and LUMO+3 (d_z^2). Fig. 4 presents the density of states (DOS) diagram for the parent complex (1) with contours of the molecular orbitals, and with the main contributions of Ru–N₂PhCH₃. As can be seen, the p_y component of the diazenido group is mostly engaged in the Ru–N₂(PhCH₃) bond (HOMO–3). The HOMO–2 contour shows electron density transfer (connected with coordination to the ruthenium metal) to the N(2) atom, which manifests in natural valence populations of the N(1) and N(2) atoms being equal to 4.76 and 5.034, respectively, as well as in natural charges (N(1) 0.211; N(2) -0.066). The electron density transfer is correlated with,

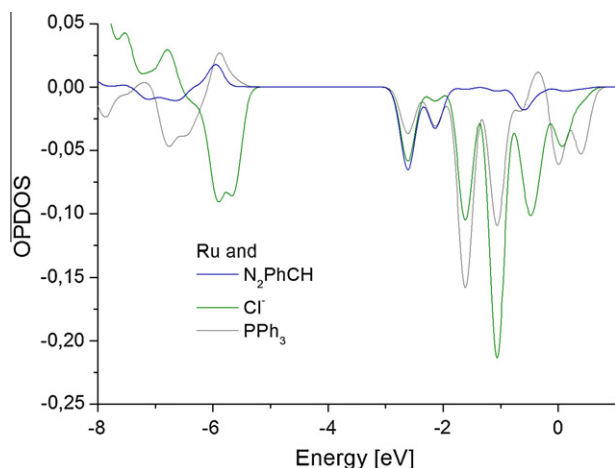


Fig. 4. The overlap partial density of states (OPDOS) diagram for the complex $[\text{RuCl}_3(\text{PPh}_3)_2(\text{N}_2\text{PhCH}_3)]$ (**2**).

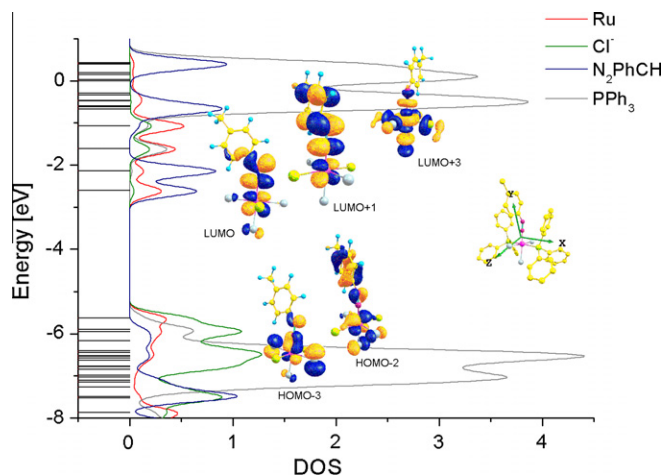


Fig. 5. The density of states (DOS) diagram for complex (**1**) with contours of the molecular orbitals describing the ruthenium *p*-tolylidiazenido ligand interaction.

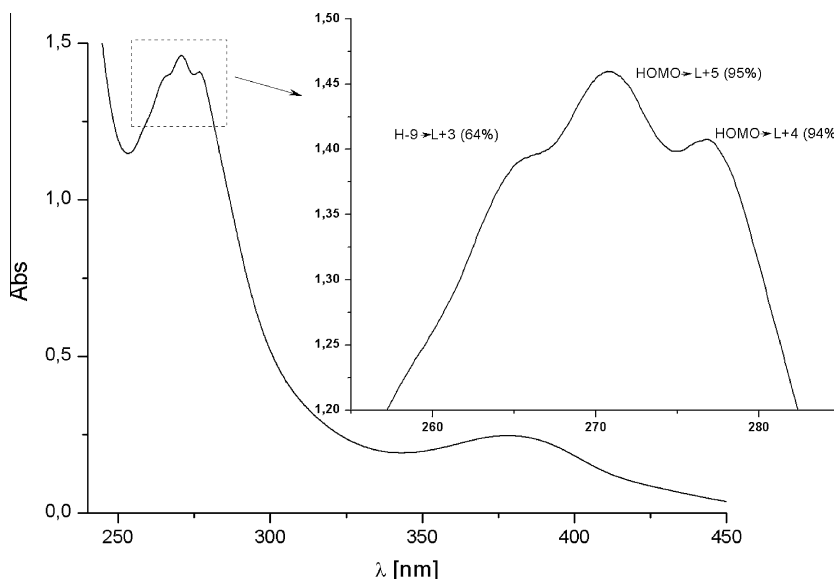


Fig. 6. UV-Vis spectrum of a methanolic solution of complex (**1**).

enabled by symmetry, interactions between ruthenium d_{π} and the Cl(2) and Cl(3) ligands (the chloride ligands lie on the *y* and *z* axes).

The participation of ruthenium *d* orbitals in the frontier HOMOs and LUMOs in complex (**1**) are in the range from 16% to 34% for HOMO–3 to HOMO and from 31 to 53% for LUMO to LUMO+3. The presence of the pyrazole or imidazole ligand in the coordination sphere of complexes (**2**) and (**3**) slightly increases the participation of the d_{Ru} orbitals in the HOMOs (19–38%) and decreases the participation in the LUMOs (15–51%). Moreover the HOMO–LUMO energy gap increases from 3.17 eV in (**1**), to 3.22 eV in (**3**) and then to 3.29 eV in complex (**2**). This change influences the luminescent properties of the complexes. Figs. 3 and 4 show that the HOMOs are composed of ruthenium *d* orbitals, with an antibonding contribution of chloride π orbitals. In turn, the *p*-tolylidiazenido ligand orbitals take part in HOMO–2 and HOMO–3 in complex (**1**) and HOMO–2/–1 in the pyrazole and imidazole complexes (**2**) and (**3**). Interestingly, the non-bonding ruthenium–diazenido ligand interaction in the parent complex (**1**) changes to bonding character in the complexes (**2**) and (**3**) with the diazole ligands (Fig. 3). The 1,2- and 1,3-diazole ligands play a meaningful role in HOMO–6, localized over the whole complex molecules with percentage participations of ruthenium and the ligands as follows: d_{Ru} (10%), PPh_3 (52–54%), Cl (7–10%), N_2PhCH_3 (8%) and pyrazole (17%) or imidazole (23%) in complexes (**2**) or (**3**), respectively. The LUMO and LUMO+1 in these complexes are localized on the ruthenium *d* orbitals (32%) and $\pi^*_{\text{N}_2\text{PhCH}_3}$ (63%) orbitals. The triphenylphosphine ligands play a role in the formation of LUMO+2, while the diazole (HPz, HIm) ligands participate in the formation of higher virtual orbitals (LUMO+10). LUMO+3 consist of the ruthenium d_{z^2} orbital as well as π^* orbitals of chloride, phosphine and *p*-tolylidiazenido ligands (see Fig. 5).

3.4. Experimental and theoretical electronic spectra

The UV–Vis spectra of the complexes are similar and present maxima in the visible part of the spectrum, in the range 437–421 nm. In the near ultraviolet region complex (**1**) presents a maximum at 374 nm, which is shifted to higher energy (304 and 308 nm) for complexes (**2**) and (**3**), of lower symmetry. In these regions, the transitions from HOMO, HOMO–2 and HOMO–7/8 to LUMO and LUMO+1 were calculated. These bands have LF (ligand field) character, but based on the participation of the ligands in

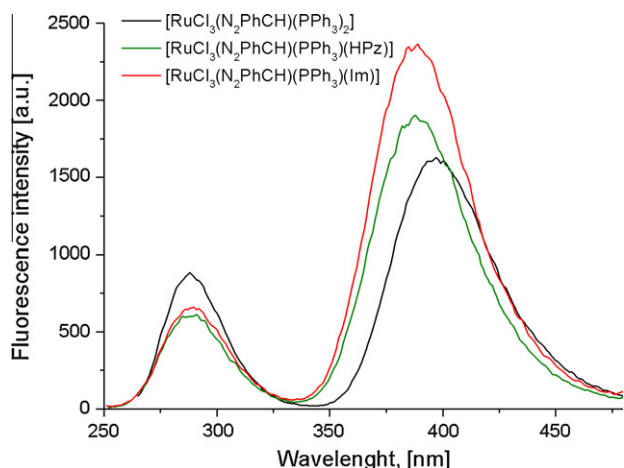


Fig. 7. The fluorescence spectra of complexes (1), (2) and (3) in methanol solutions ($c = 1 \times 10^{-4}$ mol/dm³).

these molecular orbitals MLCT (Metal–Ligand Charge Transfer) transitions also occur in the bands. The insertion of diazole ligands in complexes (2) and (3) resulted in increasing the energy of the second band associated with the participation of pyrazole and imidazole in orbitals involved in the transitions (H–7/–8 → L+1 63%; 53%). Moreover, as mentioned above, in the diazole complexes the energies of the occupied molecular orbitals decrease with the increasing energy of the unoccupied MOs, which also explains the changes in the second band positions in the UV spectrum.

In the UV region (277–261 nm) three close together bands are visible, as shown in Fig. 6. The frontier orbitals HOMO plus LUMO+4 and LUMO+5 are engaged in transitions that correspond to two bands, whilst a third band comes from the HOMO–9 → LUMO+3 transition. Based on the compositions of these orbitals, the bands have a mixed nature which can be specified by MLCT, LMCT and LLCT transitions types. Solutions of the complexes that have been excited at 258, 244 and 243 nm for complexes (1), (2) and (3), respectively, gave two emissions peaks one with a maxima close to 280 nm and a much stronger peak at 399, 385 and 389 nm, respectively. Fig. 7 presents the fluorescence spectra. The relative intensities of the emission bands are about 1.5 for (1), 4 for (2) and 5 for complex (3), thus the imidazole complex (3) gave a very intense emission. The complicated structure of the luminescence spectra suggests that more than one state is involved in the luminescence process. Hence the luminescence is of IL/MLCT origin in these systems. Probably excited molecules of these complexes undergo intersystem crossing and/or internal conversions between states and these can be luminescent. Similar emissions have been reported for a half-sandwich ruthenium complex with the 2-(2'-hydroxyphenyl)-benzoxazole ligand [56].

4. Conclusion

In summary the *p*-tolylidiazenido ruthenium(II) complex [RuCl₃(PPh₃)₂(N₂PhCH₃)], as well as new pyrazole and imidazole complexes [RuCl₃(PPh₃)(N₂PhCH₃)(L)] were synthesized and characterized by spectroscopy and X-ray crystallography. The crystal structure of complex (1) reveals non-covalent interactions between the aromatic rings and in the molecular structure of the imidazole [RuCl₃(PPh₃)(N₂PhCH₃)(Im)]·CH₃OH complex (3) an intermolecular hydrogen bonded ring is observed. The theoretical results obtained from NBO and analysis of the interactions between ruthenium and the diazenido and diazole ligands were used to explain the differences in bond lengths as well as the differences

in the IR band positions of the complexes. The donor–acceptor properties of *p*-tolylidiazenido and nitrosyl ligands were compared using the density-of-state method. The electronic structures of the complexes were characterized in particular by density-of-state diagrams. Solutions of the complexes excited in the UV spectral region gave two fluorescence maxima at 280 nm and close to 400 nm (385–399 nm).

Acknowledgement

Calculations have been carried out in Wrocław Centre for Networking and Supercomputing (<http://www.wcss.wroc.pl>).

References

- [1] J.L. Pratihār, N. Maiti, P. Pattanayak, S. Chattopadhyay, *Polyhedron* 24 (2005) 1953.
- [2] D. Banerjee, U. Ray, S. Jasimuddin, J.-C. Liou, T.-H. Lu, C. Sinha, *Polyhedron* 25 (2006) 1299.
- [3] D. Patra, J.L. Pratihār, B. Shee, P. Pattanayak, S. Chattopadhyay, *Polyhedron* 25 (2006) 2637.
- [4] P. Pratihār, A.K. Dasmahapatra, C. Sinha, *Polyhedron* 26 (2007) 1217.
- [5] T. Ren, *Chem. Rev.* 108 (2008) 4185.
- [6] T.K. Mondal, S.K. Sarker, P. Raghavaiah, C. Sinha, *Polyhedron* 27 (2008) 3020.
- [7] P. Pattanayak, J.L. Pratihār, D. Patra, V.G. Puranik, S. Chattopadhyay, *Polyhedron* 27 (2008) 2209.
- [8] J.L. Pratihār, P. Pattanayak, J.H. Huang, S. Chattopadhyay, *Inorg. Chim. Acta* 362 (2009) 5170.
- [9] D. Sardar, P. Datta, P. Mitra, C. Sinha, *Polyhedron* 29 (2010) 3170.
- [10] P. Pattanayak, D. Patra, J.L. Pratihār, A. Burrows, M. Mohan, S. Chattopadhyay, *Inorg. Chim. Acta* 363 (2010) 2865.
- [11] A.K. Sharma, S. Biswas, S.K. Barman, R. Mukherjee, *Inorg. Chim. Acta* 363 (2010) 2720.
- [12] J.L. Pratihār, P. Pattanayak, D. Patra, R. Rathore, S. Chattopadhyay, *Inorg. Chim. Acta* 367 (2011) 182.
- [13] J.L. Pratihār, P. Pattanayak, D. Patra, Chia-Her Lin, S. Chattopadhyay, *Polyhedron* 33 (2012) 67.
- [14] D. Mallick, A. Nandi, K.K. Sarker, P. Datta, T.K. Mondal, C. Sinha, *Inorg. Chim. Acta* 387 (2012) 352.
- [15] A.C.G. Hotze, M. Bacac, A.H. Velders, B.A.J. Jansen, H. Kooijman, A.L. Spek, J.G. Haasnoot, J. Reedijk, *J. Med. Chem.* 46 (2003) 1743.
- [16] A.C.G. Hotze, E.P.L. van der Geer, S.E. Caspers, H. Kooijman, A.L. Spek, J.G. Haasnoot, J. Reedijk, *Inorg. Chem.* 43 (2004) 4935.
- [17] S. Halder, R. Acharyya, S.-M. Peng, G.-H. Lee, M.G.B. Drew, S. Bhattacharya, *Inorg. Chem.* 45 (2006) 9654.
- [18] S.J. Dougan, M.M.A. Habtemariam, S. Parsons, P.J. Sadler, *Inorg. Chem.* 45 (2006) 10882.
- [19] H.-Y. Ye, F.-R. Dai, L.-Y. Zhang, Z.-N. Chen, *Inorg. Chem.* 46 (2007) 6129.
- [20] S. Kannan, R. Ramesh, Y. Liu, *J. Organomet. Chem.* 692 (2007) 3380.
- [21] S. Samanta, P. Singh, J. Fiedler, S. Žališ, W. Kaim, S. Goswami, *Inorg. Chem.* 47 (2008) 1625.
- [22] C. Renner, L. Moroder, *Chem. Biol. Chem.* 7 (2006) 868.
- [23] J. Otsuki, T. Akasaka, K. Araki, *Coord. Chem. Rev.* 252 (2008) 32.
- [24] M. Kurihara, A. Hirooka, S. Kume, M. Sugimoto, H. Nishihara, *J. Am. Chem. Soc.* 124 (2002) 8800.
- [25] K. Yamaguchi, S. Kume, K. Namiki, M. Murata, N. Tamai, H. Nishihara, *Inorg. Chem.* 44 (2005) 9056.
- [26] C.F. Barrientos-Penna, A.H. Klahn-Oliva, D. Sutton, *Organometallics* 4 (1985) 367.
- [27] A. Garcia-Minsal, D. Sutton, *Organometallics* 15 (1996) 332.
- [28] A. Cusanelli, D. Sutton, *Organometallics* 14 (1995) 4651.
- [29] A. Cusanelli, R.J. Batchelor, F.W.B. Einstein, D. Sutton, *Organometallics* 13 (1994) 5096.
- [30] C.F. Barrientos-Penna, F.W.B. Einstein, D. Sutton, A.C. Willis, *Inorg. Chem.* 19 (1980) 2740.
- [31] X. Yan, R.J. Batchelor, F.W.B. Einstein, X. Zhang, R. Nagelkerke, D. Sutton, *Inorg. Chem.* 36 (1997) 1237.
- [32] X. Yan, R.J. Batchelor, F.W.B. Einstein, D. Sutton, *Inorg. Chem.* 35 (1996) 7818.
- [33] X. Yan, F.W.B. Einstein, D. Sutton, *Can. J. Chem.* 73 (1995) 939.
- [34] G.C.-Y. Kim, R.J. Batchelor, X. Yan, F.W.B. Einstein, D. Sutton, *Inorg. Chem.* 34 (1995) 6163.
- [35] J.A. McCleverty, R.N. Whiteley, *J. Chem. Soc., Chem. Commun.* (1971) 1159.
- [36] J.A. McCleverty, D. Seddon, D.R.N. Whiteley, *J. Chem. Soc., Dalton Trans.* (1975) 839.
- [37] B.L. Haymore, J.A. Ibers, *Inorg. Chem.* 14 (1975) 3060.
- [38] B.L. Haymore, J.A. Ibers, *Inorg. Chem.* 14 (1975) 2784.
- [39] K.R. Laing, S.D. Robinson, M.F. Uttley, *J. Chem. Soc., Chem. Commun.* (1973) 176.
- [40] K.R. Laing, S.D. Robinson, M.F. Uttley, *J. Chem. Soc., Dalton Trans.* (1973) 2713.
- [41] J.V. McArdle, A.J. Schultz, B.J. Corden, R. Eisenbergi, *Inorg. Chem.* 12 (1973) 1676.

- [42] L. Fan, F.W.B. Einstein, D. Sutton, *Organometallics* 19 (2000) 684.
- [43] M.J. Frisch, G.W. Trucks, H.B. Schlegel, G.E. Scuseria, M.A. Robb, J.R. Cheeseman, G. Scalmani, V. Barone, B. Mennucci, G.A. Petersson, H. Nakatsuji, M. Caricato, X. Li, H.P. Hratchian, A.F. Izmaylov, J. Bloino, G. Zheng, J.L. Sonnenberg, M. Hada, M. Ehara, K. Toyota, R. Fukuda, J. Hasegawa, M. Ishida, T. Nakajima, Y. Honda, O. Kitao, H. Nakai, T. Vreven, J.A. Montgomery Jr., J.E. Peralta, F. Ogliaro, M. Bearpark, J.J. Heyd, E. Brothers, K.N. Kudin, V.N. Staroverov, R. Kobayashi, J. Normand, K. Raghavachari, A. Rendell, J.C. Burant, S.S. Iyengar, J. Tomasi, M. Cossi, N. Rega, J.M. Millam, M. Klene, J.E. Knox, J.B. Cross, V. Bakken, C. Adamo, J. Jaramillo, R. Gomperts, R.E. Stratmann, O. Yazyev, A.J. Austin, R. Cammi, C. Pomelli, J.W. Ochterski, R.L. Martin, K. Morokuma, V.G. Zakrzewski, G.A. Voth, P. Salvador, J.J. Dannenberg, S. Dapprich, A.D. Daniels, O. Farkas, J.B. Foresman, J.V. Ortiz, J. Cioslowski, D.J. Fox, *Gaussian 09, Revision A.1*, Gaussian, Inc., Wallingford, CT, 2009.
- [44] A.D. Becke, *J. Chem. Phys.* 98 (1993) 5648.
- [45] C. Lee, W. Yang, R.G. Parr, *Phys. Rev. B* 37 (1988) 785.
- [46] K. Eichkorn, F. Weigend, O. Treutler, R. Ahlrichs, *Theor. Chem. Acc.* 97 (1997) 119.
- [47] M.E. Casida, in: J.M. Seminario (Ed.), *Recent Developments and Applications of Modern Density Functional Theory, Theoretical and Computational Chemistry*, vol. 4, Elsevier, Amsterdam, 1996, p. 391.
- [48] E.D. Glendening, A.E. Reed, J.E. Carpenter, F. Weinhold, NBO (version 3.1), 2004.
- [49] N.M. O'Boyle, A.L. Tenderholt, K.M. Langner, *J. Comput. Chem.* 29 (2008) 839.
- [50] CrysAlis RED, Oxford Diffraction Ltd., Version 1.171.35.21, 2012.
- [51] O.V. Dolomanov, L.J. Bourhis, R.J. Gildea, J.A.K. Howard, H. Puschmann, *J. Appl. Crystallogr.* 42 (2009) 339.
- [52] G.M. Sheldrick, *Acta Crystallogr., Sect. A* 64 (2008) 112.
- [53] J.G. Małecki, M. Jaworska, R. Kruszynski, *Polyhedron* 24 (2005) 359.
- [54] G.R. Desiraju, T. Steiner, *The Weak Hydrogen Bond in Structural Chemistry and Biology*, Oxford University Press, 1999.
- [55] M.C. Etter, J.C. MacDonald, J. Bernstein, *Acta Crystallogr., Sect. B* 46 (1990) 256.
- [56] J.G. Małecki, R. Kruszynski, M. Jaworska, P. Lodowski, Z. Mazurak, *J. Organomet. Chem.* 693 (2008) 1096.